# The effect of temperature-dependent viscosity on pressure drop in axisymmetric channel flows

Marcel M. Louis,[1,*] Evgeniy Boyko,[2,†] and Howard A. Stone[1,‡]

[1] *Department of Mechanical and Aerospace Engineering, Princeton University, New Jersey 08544, USA*
[2] *Faculty of Mechanical Engineering, Technion–Israel Institute of Technology, Haifa, 3200003 Israel*

(Dated: March 23, 2024)

We investigate theoretically the influence of a temperature-dependent viscosity on the pressure drop versus flow rate relationship in pipe flows for cases where the Reynolds number is small, as expected for printing and other flows of highly viscous fluids. By applying different temperature boundary conditions at the wall, the viscosity field is altered under the same flow conditions and thus we can compare how this external heating affects the pressure drop along the length of the pipe. We use analytical and similarity-solution methods to solve for the temperature distribution under constant temperature and constant heat flux boundary conditions, as well as assumed linear and other imposed polynomial temperature versus distance (along the flow) boundary conditions at the wall. Also, for the momentum and energy equations we use the lubrication and boundary-layer approximations, respectively, which we expect to be typically appropriate for flows where the pipe radius is much less than the pipe length. The reciprocal theorem is used to derive an expression for the pressure drop across the channel for a viscosity field that depends on temperature and spatially varies across and along the flow. Assuming the fractional change in viscosity with temperature is small, we arrive at an analytical expression for the pressure drop for a given flow rate. The results are reported as a function of the effective Peclet number for each boundary condition and the numerical results are compared with analytical predictions in the low- and high-Peclet-number limits.

## I. INTRODUCTION

Viscosity gradients due to applied temperature fields in fluid flows are relevant to many natural, environmental, and industrial applications. One example is the flow of magma on a cooler surface, along which the average temperature of the fluid decreases and eventually affects the overall propagation of the current [1–6]. Additionally, extracting heavy oils from offshore sites involves pumping through the vast depths of the ocean where temperature-induced viscosity changes are inevitable [7]. In colloidal science, it has been documented that introducing temperature-induced viscosity variations in the neighborhood of the particle in a viscous fluid affects the diffusion coefficient, force, and torque experienced by the particle [8–12]. Furthermore, heat exchangers, glass fabrication, and injection molding are all examples where the working fluid experiences temperature and viscosity gradients that influence the flow behavior [13–15]. In Table I we provide a selective chronological list of previous work on pressure-driven flows in heated and/or cooled axisymmetric and two-dimensional channels. Some of the studies itemized in Table I focused on the pressure drop-flow rate relationship in channels with heated and/or cooled walls [1, 2, 15–18]. Perhaps surprisingly, no studies pertaining to the effect of the type of applied heating (i.e., boundary conditions at the wall) on the total pressure drop have been reported in the literature. In this work, we report the pressure drop as a function of an effective Peclet number for different applied temperature boundary conditions for cases where the relative change in viscosity is small.

Various pressure drop-flow rate relations have been reported over the years. For example, for small variations in viscosity with temperature and pressure in axisymmetric channel flows with isothermal and adiabatic boundaries, the effects of viscous heating were derived in [16]. Also, steady flows in heated and cooled channels driven by a constant mass flux were studied with a focus on the temperature and velocity fields in the high viscosity variation limits, for exponential and algebraic viscosity dependence with temperature [17]. The study was extended to polymer melts flowing through ducts with heated walls, where viscous heating effects were included [18]. Geophysical applications involving magma motivate some work, such as the case where viscosity varied linearly with temperature [1]. Also, the flow of hot viscous fluid on a cooled constant temperature wall was studied by Wylie and Lister [2], who employed numerical techniques to determine the pressure drop-flow rate relationship in the limit where viscosity variations are

* mmlouis@princeton.edu
† evgboyko@technion.ac.il
‡ hastone@princeton.edu

| Year | Authors | Source of heat considered | Geometry | Reported $\mu(T)$ effect on |
|---|---|---|---|---|
| 1975 | Galili *et al.* [16] | Isothermally heated walls and viscous heating | Pipe | Pressure drop-flow rate relation |
| 1977 | Ockendon and Ockendon [17] | Isothermally heated and cooled walls | 2-D channel | Velocity and pressure fields |
| 1977 | Pearson [19] | Viscous heating | 2-D channel | Temperature, velocity, and pressure drop |
| 1978 | Ockendon [20] | Viscous heating | 2-D channel | Velocity, pressure fields and boundary layer |
| 1981 | Denn [21] | Viscous heating | Pipe | Pressure drop-flow rate relation |
| 1986 | Richardson [15] | Isothermally heated walls | 2-D channel, pipe and disk | Pressure drop-flow rate relation |
| 1987 | Richardson [18] | Isothermally heated walls | 2-D channel, pipe, and disk | Pressure drop-flow rate relation and thermal boundary layer |
| 1988 | Sun [22] | Isothermally heated and cooled walls with viscous heating | 2-D channel | Temperature and velocity fields |
| 1991 | Whitehead and Helfrich [1] | Isothermally heated walls | 1-D and 2-D channel | Pressure drop and flow stability |
| 1993 | Schäfer and Herwig [23] | Constant flux at walls | 2-D channel | Poisieulle flow stability |
| 1995 | Wylie and Lister [2] | Isothermally heated walls | 2-D channel | Pressure drop-flow rate relation and flow stability |
| 2002 | Costa and Macedonio [4] | Viscous heating | 2-D channel | Flow stability |
| 2005 | Costa and Macedonio [5] | Viscous heating | 2-D channel | Flow stability |

TABLE I. Chronological selection of previous experimental, numerical, and theoretical works on the low-Reynolds-number pressure-driven flows in heated and/or cooled two-dimensional and axisymmetric geometries for Newtonian and non-Newtonian fluids.

high and confirmed the bifurcations previously reported by Whitehead and Helfrich [1]. Additionally, they investigated flow stability and found that fingering-like structures develop at high viscosity variations.

In this work, we present an analytical expression for the total pressure drop for a given flow rate across an axisymmetric channel for various prescribed temperature boundary conditions at the wall. Utilizing the Lorentz reciprocal theorem, we circumvent the coupled hydrodynamic-heat transfer problem in the lubrication limit. Specifically, we linearize the viscosity distribution and obtain the first-order correction to the total pressure drop. Previous studies have approached this problem by applying isothermal heating or cooling conditions at the wall and solving the resultant total pressure drop. However, in practice, wall temperatures never truly conform to isothermal conditions. Therefore, we extend this approach by applying constant flux and linear boundary conditions (i.e., temperature as a function of downstream position) to the classical Graetz equation from which we obtain analytical solutions for the temperature field. By re-scaling the velocity field with the average velocity thereby keeping the mass flux fixed, we elucidate the influence of the effective Peclet number (defined in Sec. V) on the average temperature in the fluid domain. Furthermore, we study the effect of the applied temperature conditions at the wall on the first-order pressure drop correction as a function of effective Peclet number. When analyzing the high-Peclet-number limit, we take advantage of the Lévêque equation to approximate the temperature field for different boundary conditions and show that our results for the pressure drop obtained from the Lévêque approach are in excellent agreement with the Graetz approximation. To our knowledge, we are not aware of any approach that encapsulates the effect the nature of the applied heating has on the total pressure drop in the form of a comparison as we aim to report in this study.

## II. LUBRICATION SCALING OF MASS AND MOMENTUM EQUATIONS

We consider an incompressible steady flow of a Newtonian fluid in an axisymmetric channel of radius $r_0$ and length $\ell$, where $r_0 \ll \ell$, as shown in Fig. 1. A temperature boundary condition is applied at the walls of the channel ($r = r_0$), which induces a viscosity distribution throughout the fluid domain since viscosity is a function of temperature. The fluid motion is assumed to remain laminar and is described by a velocity $\mathbf{u} = (u_z, u_r)$ and a pressure distribution $p$ due to an applied flow rate $q$. Our main goal is to determine the overall pressure drop $\Delta p$ and how the thermal boundary condition influences the results.

We start by outlining a lubrication-style description of the governing equations in the low-Reynolds-number limit but allowing for convective effects in the thermal energy equation. In our analysis, we neglect buoyancy-driven

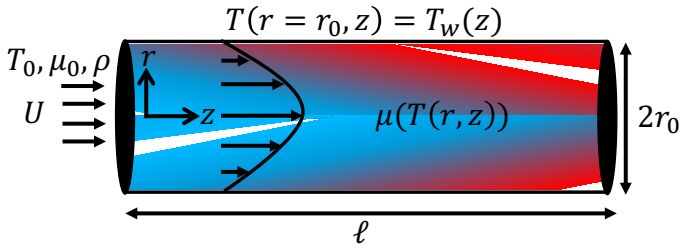


FIG. 1. A fluid enters an axisymmetric channel with temperature $T_0$ and viscosity $\mu_0$; $\rho$ is the fluid density. The temperature at the wall, $T_w(z)$, is different from $T_0$ and may vary along the length of the channel, resulting in temperature and viscosity gradients throughout the fluid domain.

contributions, which may arise from density variations with temperature, and thus change the flow field. Comparing the ratio of the characteristic velocity due to buoyancy forces, $O(\Delta\rho g r_0^2/\mu_0)$, to the characteristic velocity that drives the flow, $O(q/r_0^2)$, we find the ratio $\Delta\rho g r_0^4/q\mu_0$ representing the relative importance of buoyancy effects, where $\Delta\rho$ is the magnitude of density changes from the mean density $\rho$ and $g$ is the acceleration of gravity in the axial direction. When this ratio is small, $\Delta\rho g r_0^4/q\mu_0 \ll 1$, the buoyancy has a negligible influence on the flow field, and the temperature variations are incorporated only through the variation of the viscosity. Under the above condition, the fluid motion is described by the continuity and Cauchy momentum equations:

$$\boldsymbol{\nabla}\cdot\mathbf{u} = 0, \qquad \boldsymbol{\nabla}\cdot\boldsymbol{\sigma} = \mathbf{0}, \tag{1}$$

where $\boldsymbol{\sigma}$ is the stress tensor for a Newtonian fluid, which takes the form:

$$\boldsymbol{\sigma} = -p\mathbf{I} + 2\mu(T)\mathbf{E}. \tag{2}$$

Here $\mathbf{I}$ is the identity tensor and $\mathbf{E} = (1/2)(\nabla\mathbf{u} + (\nabla\mathbf{u})^T)$ is the rate-of-strain tensor. The stress tensor involves a temperature-dependent viscosity, $\mu(T)$, where the temperature field is a function of $r$ and $z$. Hence, we have

$$-\boldsymbol{\nabla}p + \boldsymbol{\nabla}\cdot\left[\mu(r,z)(\boldsymbol{\nabla}\mathbf{u} + \boldsymbol{\nabla}\mathbf{u}^T)\right] = \mathbf{0}, \tag{3}$$

where we have neglected buoyancy-driven contributions as mentioned above.

To solve the mass and momentum equations, we impose no-slip and no-penetration boundary conditions at $r = r_0$ and apply an integral constraint for the flow rate, $2\pi\int_0^{r_0} u_z r dr = q$, where we have neglected volumetric variations due to density changes with temperature. For convenience, we choose the characteristic velocity scale as $\bar{U} = q/(2\pi r_0^2)$, which ensures that the non-dimensional integral constraint for volume flux is equal to 1.

Therefore, we nondimensionalize the governing equations by applying lubrication theory and using the dimensionless variables:

$$Z = \frac{z}{\ell}, \quad R = \frac{r}{r_0}, \quad U_r = \frac{u_r}{\epsilon q/2\pi r_0^2}, \quad U_z = \frac{u_z}{q/2\pi r_0^2}, \quad P = \frac{p}{\mu_0 q\ell/2\pi r_0^4}, \quad \mathcal{M} = \frac{\mu(r,z)}{\mu_0}, \tag{4}$$

where $\epsilon = r_0/\ell$ is the aspect ratio, which we assume to be small, $\epsilon \ll 1$, and $\mathcal{M}(r,z)$ is the dimensionless viscosity. Applying the rescaling to Eqs. (1) and (2), we arrive at

$$\frac{1}{R}\frac{\partial(RU_r)}{\partial R} + \frac{\partial U_z}{\partial Z} = 0, \qquad \frac{\partial P}{\partial Z} = \frac{1}{R}\frac{\partial}{\partial R}\left(R\mathcal{M}(R,Z)\frac{\partial U_z}{\partial R}\right) + O(\epsilon^2), \qquad \frac{\partial P}{\partial R} = O(\epsilon^2). \tag{5}$$

From Eq. (5), it follows that $P = P(Z) + O(\epsilon^2)$, i.e., the pressure is independent of $R$ up to $O(\epsilon^2)$, consistent with the classical lubrication approximation. We note that in the next sections, we bypass using the lubrication equations (5) to solve the hydrodynamic and heat transfer problems and use instead the reciprocal theorem.

## III. RECIPROCAL THEOREM FOR FLOWS WITH NON-UNIFORM VISCOSITY IN AXISYMMETRIC NARROW CHANNELS

The Lorentz reciprocal theorem is a useful tool that can be applied to fluid dynamics and transport phenomenon problems to calculate integral quantities, such as force, torque, pressure drop, and flow rate, while bypassing detailed

calculations of primary quantities [24]. We outline a model problem by defining $\hat{\mathbf{u}}$ and $\hat{\boldsymbol{\sigma}}$ as the velocity and stress fields that correspond to the case in which there are no temperature variations in the system. In this model, the entrance viscosity, $\mu_0$, remains constant over the entire fluid domain. Therefore, the respective mass and momentum equations are

$$\boldsymbol{\nabla}\cdot\hat{\mathbf{u}}=0, \qquad \boldsymbol{\nabla}\cdot\hat{\boldsymbol{\sigma}}=\mathbf{0} \qquad \text{where} \qquad \hat{\boldsymbol{\sigma}}=-\hat{p}\mathbf{I}+2\mu_0\hat{\mathbf{E}}. \tag{6}$$

Following standard steps, we arrive at the reciprocal theorem in the form:

$$\int_{S_0}\mathbf{n}\cdot\boldsymbol{\sigma}\cdot\hat{\mathbf{u}}\,\mathrm{d}S+\int_{S_\ell}\mathbf{n}\cdot\boldsymbol{\sigma}\cdot\hat{\mathbf{u}}\,\mathrm{d}S-\int_{S_0}\mathbf{n}\cdot\hat{\boldsymbol{\sigma}}\cdot\mathbf{u}\,\mathrm{d}S-\int_{S_\ell}\mathbf{n}\cdot\hat{\boldsymbol{\sigma}}\cdot\mathbf{u}\,\mathrm{d}S=2\int_V(\mu(T)-\mu_0)\mathbf{E}\,:\,\hat{\mathbf{E}}\,\mathrm{d}V, \tag{7}$$

where $V$ is the fluid volume and $\mathbf{n}$ is the unit outward normal corresponding to the cross-sectional surfaces at the beginning and end of the channel $S_{0,\ell}$. We also take advantage of the no-slip boundary conditions at the walls so that the surface integrals vanish there. Recently, a similar approach has been used to calculate the pressure drop of non-Newtonian fluid flow in narrow geometries [25, 26].

Next, we rescale the variables in the surface and volume integrals according to Eq. (4), using similar definitions for the hat variables, and find

$$2(\mu(T)-\mu_0)\mathbf{E}:\hat{\mathbf{E}}=\frac{q^2\mu_0}{4\pi^2r_0^6}\left[(\mathcal{M}-1)\frac{\partial U_z}{\partial R}\frac{\partial\hat{U}_z}{\partial R}+O(\epsilon^2)\right], \tag{8a}$$

$$\mathbf{n}\cdot\boldsymbol{\sigma}\cdot\hat{\mathbf{u}}=\mp\frac{\mu_0q^2\ell}{4\pi^2r_0^6}[-P\hat{U}_z+O(\epsilon^2)], \tag{8b}$$

$$\mathbf{n}\cdot\hat{\boldsymbol{\sigma}}\cdot\mathbf{u}=\mp\frac{\mu_0q^2\ell}{4\pi^2r_0^6}[-\hat{P}U_z+O(\epsilon^2)], \tag{8c}$$

where the minus and plus signs correspond to $S_0$ and $S_\ell$, respectively; recall that $\mathcal{M}$ is the dimensionless viscosity. Combining terms and simplifying Eq. (7), we obtain:

$$\int_0^1(P\hat{U}_z)R|_{Z=0}\mathrm{d}R-\int_0^1(P\hat{U}_z)R|_{Z=1}\mathrm{d}R-\int_0^1(\hat{P}U_z)R|_{Z=0}\mathrm{d}R+\int_0^1(\hat{P}U_z)R|_{Z=1}\mathrm{d}R=\int_0^1\int_0^1(\mathcal{M}-1)R\frac{\partial U_z}{\partial R}\frac{\partial\hat{U}_z}{\partial R}\mathrm{d}R\mathrm{d}Z+O(\epsilon^2). \tag{9}$$

Because of our choice for the velocity scale, then $\int_0^1 U_zR\,\mathrm{d}R=\int_0^1\hat{U}_zR\,\mathrm{d}R=1$. Additionally, we define the pressure drops $\Delta P=P(0)-P(1)$ and $\Delta\hat{P}=\hat{P}(0)-\hat{P}(1)$ so that, upon further simplification, we obtain the expression for the pressure drop

$$\Delta P-\Delta\hat{P}=\int_0^1\int_0^1(\mathcal{M}-1)R\frac{\partial U_z}{\partial R}\frac{\partial\hat{U}_z}{\partial R}\,\mathrm{d}R\mathrm{d}Z+O(\epsilon^2). \tag{10}$$

## IV. LINEARIZATION OF THE VISCOSITY FIELD AND PERTURBATION ANALYSIS

In order to characterize an approximate variation in the viscosity, we expand the viscosity into a Taylor series around the inlet temperature $T_0$, corresponding to the viscosity $\mu_0$. We also introduce a dimensionless variable for temperature, $\Theta(R,Z)=(T(r,z)-T_0)/\Delta T$, where $\Delta T$ is determined by the boundary conditions. The corresponding expansion for the viscosity is

$$\mathcal{M}=\frac{\mu(T)}{\mu_0}=1+\frac{\Delta T}{\mu_0}\left.\frac{\partial\mu}{\partial T}\right|_{T_0}\Theta(R,Z)+\frac{(\Delta T)^2}{2\mu_0}\left.\frac{\partial^2\mu}{\partial T^2}\right|_{T_0}[\Theta(R,Z)]^2+\cdots \tag{11}$$

We expect that $\partial\mu/\partial T < 0$ and so define the parameter $\beta$ that represents the fractional change of viscosity,

$$\beta = -\frac{\Delta T}{\mu_0}\left.\frac{\partial \mu}{\partial T}\right|_{T_0}. \tag{12}$$

For $\beta \ll 1$, Eq. (11) becomes

$$\mathcal{M}(\Theta) \approx 1 - \beta\Theta + O(\beta^2). \tag{13}$$

Substituting Eq. (13) into Eq. (10), we obtain

$$\Delta P = \Delta \hat{P} - \beta \int_0^1 \int_0^1 \Theta R \frac{\partial U_z}{\partial R}\frac{\partial \hat{U}_z}{\partial R} \mathrm{d}R\mathrm{d}Z + O(\epsilon^2, \beta^2). \tag{14}$$

To simplify further, we expand the pressure drop and velocity into perturbation series in the dimensionless parameter $\beta \ll 1$ by defining $U_z = U_{z,0} + \beta U_{z,1} + O(\beta^2)$ and $\Delta P = \Delta P_0 + \beta \Delta P_1 + O(\beta^2)$. Using the latter expansions and noting that $\Delta \hat{P} = \Delta P_0$ and $\hat{U}_z = U_{z,0} = 4(1 - R^2)$, we obtain the expression for the first-order pressure drop correction

$$\Delta P_1 = -\int_0^1 \int_0^1 \Theta R \left(\frac{\partial \hat{U}_z}{\partial R}\right)^2 \mathrm{d}R\mathrm{d}Z = -64 \int_0^1 \int_0^1 \Theta(R, Z) R^3 \mathrm{d}R\mathrm{d}Z. \tag{15}$$

Equation (15) is the central result of this work, which allows the determination of the first-order correction to the pressure drop of the heated channel, provided the temperature distribution $\Theta(R, Z)$ is known. Particularly, Eq. (15) highlights that small changes in viscosity allow us to bypass the coupled hydrodynamic heat transfer problem to calculate the leading-order pressure drop correction. Instead, we can find the temperature distribution from the energy equation using the constant viscosity velocity field and then use it to calculate the pressure drop using Eq. (15).

## V. ENERGY EQUATION: LUBRICATION RESCALING AND SOLUTIONS

Next, we rescale the energy equation. At the leading order in $\beta$, the flow is unidirectional and not a function of the axial direction. Thus, the vertical velocity is zero, i.e., $U_{r,0} \equiv 0$. Similar to the velocity and pressure drop, we expand the temperature as $\Theta = \Theta_0 + \beta\Theta_1 + O(\beta^2)$ and obtain the dimensionless energy equation at leading order:

$$\epsilon Pe \left(U_{z,0}\frac{\partial \Theta_0}{\partial Z}\right) = \frac{1}{R}\frac{\partial}{\partial R}\left(R\frac{\partial \Theta_0}{\partial R}\right) + \epsilon^2 \frac{\partial^2 \Theta_0}{\partial Z^2}, \tag{16}$$

where we define the Peclet number $Pe = \bar{U} r_0/\alpha$ with $\bar{U} = q/(2\pi r_0^2)$ the characteristic velocity as previously defined in Sec. II, and $\alpha$ the thermal diffusivity. We can neglect axial conduction, which is $O(\epsilon^2)$, as long as $Pe \gg \epsilon$, consistent with the lubrication limit ($\epsilon \ll 1$). We also introduce the effective Peclet number, $Pe_{\text{eff}} = \epsilon Pe$. Noting that $U_{z,0} = 4(1 - R^2)$ and dropping the subscript 0 for convenience, we thus consider the Graetz equation in the form:

$$4Pe_{\text{eff}}(1 - R^2)\frac{\partial \Theta}{\partial Z} = \frac{1}{R}\frac{\partial}{\partial R}\left(R\frac{\partial \Theta}{\partial R}\right), \tag{17}$$

which was originally solved by Graetz [27, 28] and later extended to include axial conduction and viscous dissipation effects [29–31]. In this section, we solve Eq. (17) by applying boundary conditions at the wall for constant temperature, constant thermal flux, and a linear temperature variation in the axial direction. We obtain results for the temperature field for different effective Peclet numbers. In Sec. V D, we will show how the Lévêque approximation [32] simplifies Eq. (17) to yield a self-similar solution, which allows an analytical expression for the pressure drop for a range of effective Peclet numbers.

### A. Temperature field with Dirichlet boundary conditions applied at the wall

First, we solve Eq. (17) using Dirichlet boundary conditions at the wall, where $T = T_w > T_0$ and choose $\Delta T = T_w - T_0$. In dimensionless variables, the boundary conditions are $\Theta(R = 1, Z) = 1$, $\Theta(R = 0, Z) =$ finite and

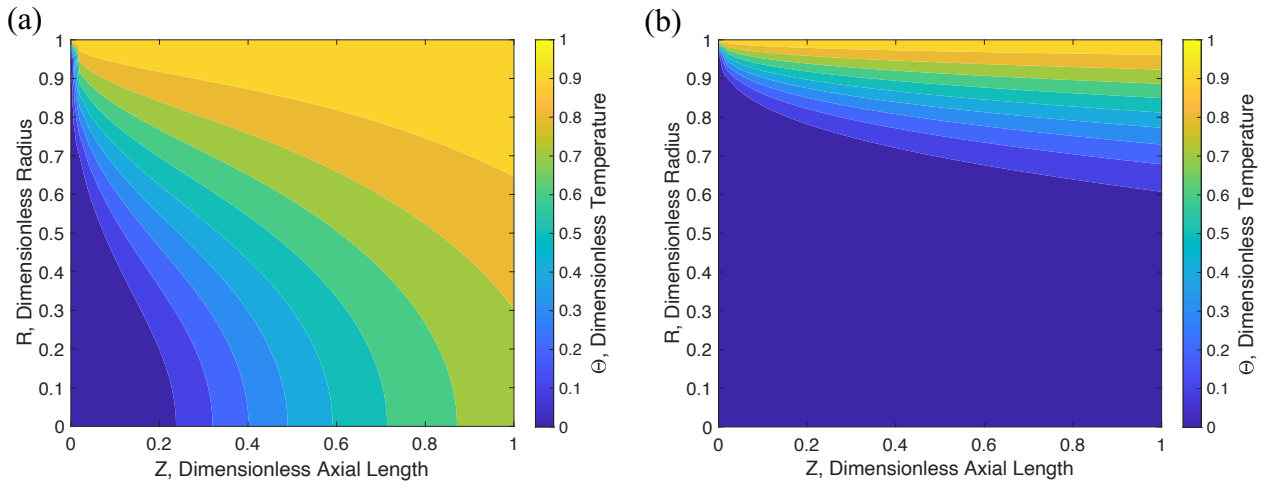


FIG. 2. Contour plot of the temperature distribution due to applied boundary condition $\Theta(R=1,Z)=1$: (a) $Pe_{\text{eff}}=1$ and (b) $Pe_{\text{eff}}=25$.

$\Theta(R,Z=0)=0$ and we solve Eq. (17) for $\Theta$, which leads to:

$$\Theta(R,Z)=1-\sum_{n=1}^{\infty}A_n\exp\left[-\frac{\lambda_n^2 Z}{4Pe_{\text{eff}}}\right]\exp\left[-\frac{\lambda_n R^2}{2}\right]{}_1F_1\left[\frac{1}{2}-\frac{\lambda_n}{4},1,\lambda_n R^2\right], \tag{18a}$$

$$\text{Eigenvalue condition:}\quad {}_1F_1\left[\frac{1}{2}-\frac{\lambda_n}{4},1,\lambda_n\right]=0, \tag{18b}$$

$$A_n=\frac{\int_0^1 R(1-R^2)\exp\left[-\frac{\lambda_n R^2}{2}\right]{}_1F_1\left[\frac{1}{2}-\frac{\lambda_n}{4},1,\lambda_n R^2\right]\mathrm{d}R}{\int_0^1 R(1-R^2)\left(\exp\left[-\frac{\lambda_n R^2}{2}\right]{}_1F_1\left[\frac{1}{2}-\frac{\lambda_n}{4},1,\lambda_n R^2\right]\right)^2\mathrm{d}R}. \tag{18c}$$

Here ${}_1F_1[a,b,c]$ is the confluent hypergeometric function and $\lambda_n$ are the eigenvalues that are found by finding the zeros of Eq. (18b). The corresponding constants $\{A_n\}$ are found using the boundary condition at the inlet and orthogonality of the eigenfunctions, as shown in Eq. (18c).

Typical results for the temperature distribution, presented as contour plots of $\Theta(R,Z)$, for $Pe_{\text{eff}}=1$ and $Pe_{\text{eff}}=25$, are shown in Fig. 2. When $Pe_{\text{eff}}\ll 1$, we approach the limit where the temperature at the wall has time to conduct throughout much of the fluid domain relative to the advective timescale, which leaves only a small region at the inlet with a temperature different from unity. In contrast, when $Pe_{\text{eff}}\gg 1$, the lower temperature fluid at the inlet is advected effectively throughout the channel. Subsequently, a boundary layer develops near the wall where the temperature varies from the bulk temperature. In this limit, the bulk fluid has a temperature, $\Theta=0$ as shown in Fig 2(b). As expected, the thickness of this boundary layer decreases as $Pe_{\text{eff}}$ increases.

### B. Temperature field with a constant flux condition applied at the wall

Next, we apply a constant heat flux $q_0$ as the boundary condition at the wall to solve Eq. (17). In dimensionless terms, the boundary conditions become $\partial\Theta/\partial R(R=1,Z)=1$, $\Theta(R=0)=$ finite, and $\Theta(Z=0)=0$. In this case, $\Delta T=q_0 r_0/k$, where $k$ is the thermal conductivity. Solving Eq. (17) using similar techniques as in the previous subsection, we obtain:

$$\Theta(R,Z)=\sum_{n=1}^{\infty}B_n\exp\left[-\frac{\lambda_n^2 Z}{4Pe_{\text{eff}}}\right]\exp\left[-\frac{\lambda_n R^2}{2}\right]{}_1F_1\left[\frac{1}{2}-\frac{\lambda_n}{4},1,\lambda_n R^2\right]+\frac{Z}{Pe_{\text{eff}}}+\left(R^2-\frac{R^4}{4}\right), \tag{19a}$$

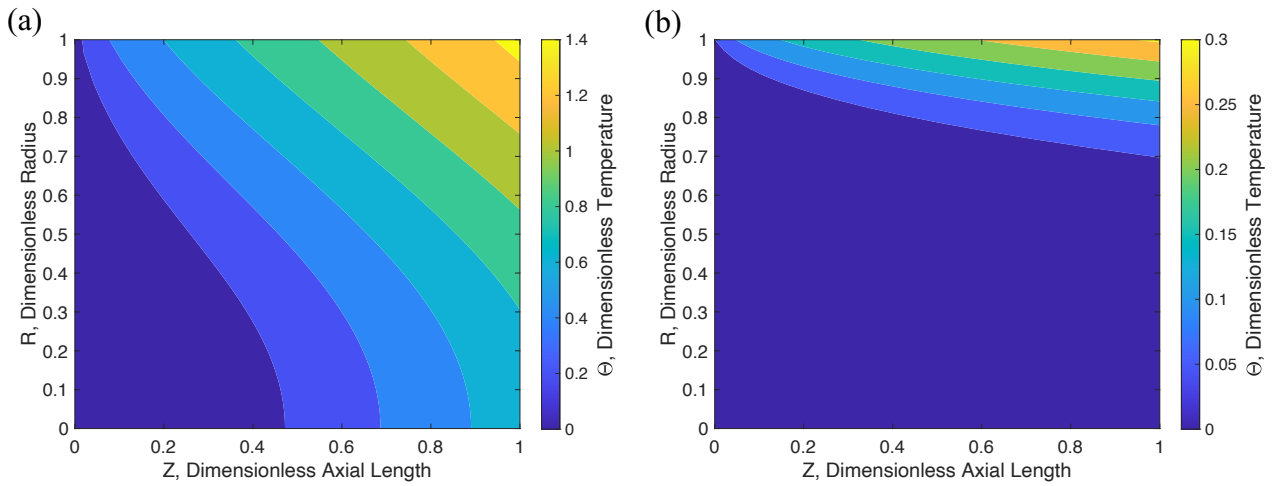


FIG. 3. Contour plot of the temperature distribution due to applied boundary condition $\frac{\partial\Theta}{\partial R}(R=1,Z)=1$: (a) $Pe_{\text{eff}}=1$ and (b) $Pe_{\text{eff}}=25$.

$$\text{Eigenvalue condition:}\quad 2\left(\frac{1}{2}-\frac{\lambda_n}{4}\right){}_1F_1\left[\frac{3}{2}-\frac{\lambda_n}{4},2,\lambda_n\right]-{}_1F_1\left[\frac{1}{2}-\frac{\lambda_n}{4},1,\lambda_n\right]=0, \tag{19b}$$

$$B_n=\frac{\int_0^1\left(\frac{1}{4}R^4-R^2\right)R(1-R^2)\exp\left[-\frac{\lambda_nR^2}{2}\right]{}_1F_1\left[\frac{1}{2}-\frac{\lambda_n}{4},1,\lambda_nR^2\right]\mathrm{d}R}{\int_0^1 R(1-R^2)\left(\exp\left[-\frac{\lambda_nR^2}{2}\right]{}_1F_1\left[\frac{1}{2}-\frac{\lambda_n}{4},1,\lambda_nR^2\right]\right)^2\mathrm{d}R}, \tag{19c}$$

where the eigenvalues were found by calculating the zeros of Eq. (19b) and the corresponding constants $\{B_n\}$ are found by using the boundary condition at the inlet by applying the orthogonality of the eigenfunctions, as shown in Eq. (19c).

Typical results for $\Theta(R,Z)$ are shown in Fig. 3 in the form of a contour plot for $Pe_{\text{eff}}=1$ and $Pe_{\text{eff}}=25$. Unlike the constant temperature boundary condition case, the constant flux boundary condition does not constrain a fixed temperature at the wall. In this case, $Pe_{\text{eff}}$ affects both the wall temperature (where the temperature in the fluid is maximum), and the boundary layer thickness, which both influence the average temperature in the flow. When $Pe_{\text{eff}}\gg 1$, the maximum temperature in the fluid domain is approximately zero, whereas when $Pe_{\text{eff}}\ll 1$, a constant wall heat flux increases the average temperature in the flow field (and along the wall), as shown by the second term in Eq. (19a). For example in Fig. 3, the maximum temperature for $Pe_{\text{eff}}=25$ is less than $Pe_{\text{eff}}=1$, in addition to the aforementioned boundary layer thickness-effective Peclet number relationship. This unique coupling suggests a stronger correlation between the pressure drop correction term and $Pe_{\text{eff}}$ in the low and high-$Pe_{\text{eff}}$ limit compared to other applied boundary conditions (see Fig. 7(a)).

### C. Temperature field with linear boundary condition applied at the wall

We study yet another configuration by imposing a linear temperature variation at the wall: $T(r=r_0,z)=\mathcal{B}z+T_0$. We rescale $\Theta$ such that $\Delta T=\mathcal{B}\ell$ where $\ell$ is the length of the tube and $\mathcal{B}$ is the slope of the linear profile. The rescaled boundary conditions are $\Theta(R=1,Z)=Z$, $\Theta(0,Z)=$ finite and $\Theta(R,Z=0)=0$. Using these boundary conditions, the solution of Eq. (17) for $\Theta(R,Z)$ is

$$\Theta(R,Z)=\sum_{n=1}^{\infty}C_n\exp\left[-\frac{\lambda_n^2Z}{4Pe_{\text{eff}}}\right]\exp\left[-\frac{\lambda_nR^2}{2}\right]{}_1F_1\left[\frac{1}{2}-\frac{\lambda_n}{4},1,\lambda_nR^2\right]+Z+\frac{Pe_{\text{eff}}}{4}(R^4-4R^2+3), \tag{20a}$$

$$C_n=\left(\frac{Pe_{\text{eff}}}{4}\right)\frac{\int_0^1\left(4R^2-R^4-3\right)R(1-R^2)\exp\left[-\frac{\lambda_nR^2}{2}\right]{}_1F_1\left[\frac{1}{2}-\frac{\lambda_n}{4},1,\lambda_nR^2\right]\mathrm{d}R}{\int_0^1 R(1-R^2)\left(\exp\left[-\frac{\lambda_nR^2}{2}\right]{}_1F_1\left[\frac{1}{2}-\frac{\lambda_n}{4},1,\lambda_nR^2\right]\right)^2\mathrm{d}R}. \tag{20b}$$

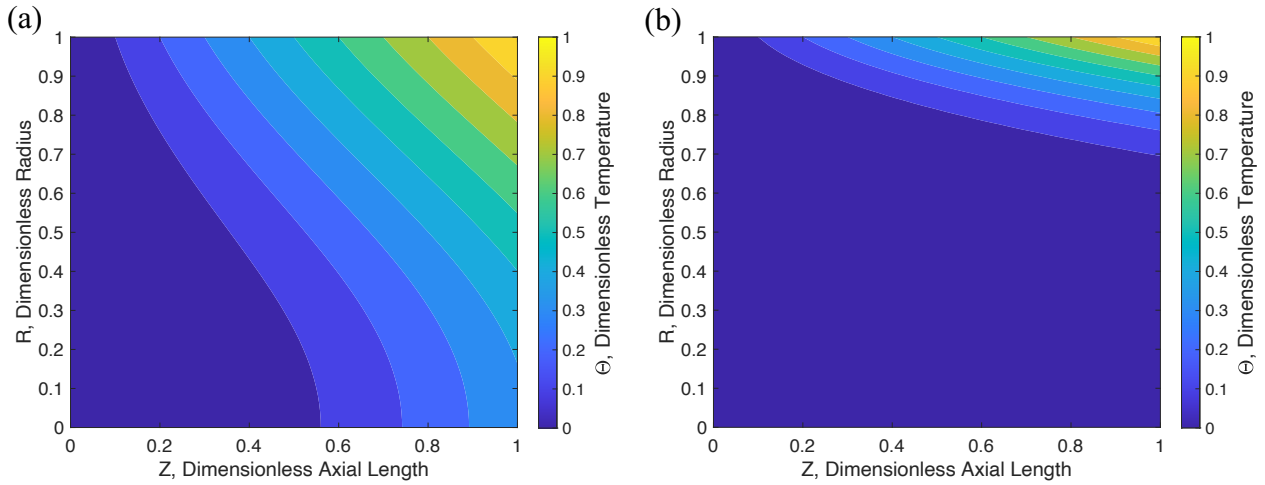


FIG. 4. Contour plot of the temperature distribution due to applied boundary condition $\Theta(R=1)=Z$: (a) $Pe_{\text{eff}}=1$ and (b) $Pe_{\text{eff}}=25$.

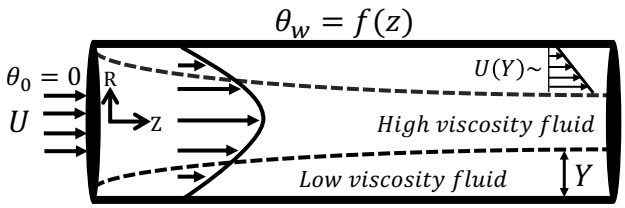


FIG. 5. In the $Pe_{\text{eff}} \gg 1$ limit, a cooler fluid with higher viscosity is advected across the channel length, leaving a small region of warmer-lower-viscosity fluid near the wall.

The eigenvalues were found by calculating the zeros of Eq. (18b) shown previously and the corresponding constants $\{C_n\}$ are found by using the boundary condition at the inlet by applying the orthogonality of the eigenfunctions, as shown in Eq. (20b).

In Figs. 4(a,b), we show the contours of the dimensionless temperature distribution $\Theta(R,Z)$ for (a) $Pe_{\text{eff}}=1$ and (b) $Pe_{\text{eff}}=25$. When conduction is dominant, $Pe_{\text{eff}} \ll 1$, there is approximately a linear increase in temperature as a function of axial direction for all $R$, mimicking the wall temperature. Therefore, the average temperature in the fluid domain will always be less than the applied Dirichlet-boundary-condition case for a given $Pe_{\text{eff}}$. When $Pe_{\text{eff}} \gg 1$, the temperature in the boundary layer monotonically increases with $Z$ in accordance to the wall temperature; while its thickness decreases with $Pe_{\text{eff}}$, as shown previously. Such a decreasing boundary-layer thickness with increasing $Pe_{\text{eff}}$ is consistent among the three boundary conditions we considered, motivating us to investigate an approximation to Eq. (17) in the limit where the effective Peclet number is sufficiently high.

### D. Lévêque approximations in the high-effective-Peclet-number limit

For $Pe_{\text{eff}} \gg 1$, we identify a narrow boundary-layer region of thickness $Y$, where the temperature is non-zero and the fluid has a lower viscosity, as shown in Fig 5. Outside this narrow region, the fluid has a temperature $\Theta=0$ and a higher viscosity. By letting $R=1-Y$ where $Y \ll 1$, the velocity within the boundary layer can be expressed as $U_{z,0}=4Y(2+Y)\approx 8Y$, so that the velocity profile is approximately linear. Applying the latter result to Eq. (17), we obtain the well-known Lévêque equation [32]

$$8Pe_{\text{eff}} Y \frac{\partial \Theta}{\partial Z} = \frac{\partial^2 \Theta}{\partial Y^2}, \tag{21}$$

which has a known similarity solution for Dirichlet boundary conditions. Here we apply the boundary condition: $\Theta(R=1) = Z^{\alpha}$. Next, we seek a solution of the form: $\Theta(\eta) = Z^{\alpha} f(\eta)$, where $\eta = 2Pe_{\text{eff}}^{\frac{1}{3}} Y/Z^{\frac{1}{3}}$. Substituting this ansatz into Eq. (21) yields the ordinary differential equation (ODE):

$$3f''(\eta) + \eta^2 f'(\eta) - 3\alpha\eta f(\eta) = 0. \tag{22}$$

Equation (22) has a solution for different values of $\alpha$ as long as $\alpha \geq 0$ subject to the conditions $f(\eta \to \infty) = 0$ and $f(\eta = 0) = 1$. For example, when $\alpha = 0$ we find the following solution for $f(\eta)$:

$$f(\eta) = \frac{\Gamma[\frac{1}{3}, \frac{\eta^3}{9}]}{\Gamma[\frac{1}{3}]} = \frac{1}{\Gamma[\frac{1}{3}]} \int_{\eta^3/9}^{\infty} t^{-\frac{2}{3}} \exp(-t) \mathrm{d}t, \tag{23}$$

where $\Gamma[.]$ is the Gamma function and $\Gamma[.,.]$ is the incomplete Gamma function.

We also extend this approach by applying the constant flux condition, for which we substitute $\Theta(\eta) = \frac{1}{2} Pe_{\text{eff}}^{-\frac{1}{3}} Z^{\frac{1}{3}} f(\eta)$ into Eq. (21), leading to the ODE:

$$3f''(\eta) + \eta^2 f'(\eta) - \eta f(\eta) = 0, \tag{24}$$

subject to $f'(\eta = 0) = -1$ and $f(\eta \to \infty) = 0$. The corresponding solution in this case is

$$f(\eta) = \frac{\eta\Gamma[-\frac{1}{3}, \frac{\eta^3}{9}]}{3\Gamma[\frac{2}{3}]} = \frac{\eta}{3\Gamma[\frac{2}{3}]} \int_{\eta^3/9}^{\infty} t^{-\frac{4}{3}} \exp(-t) \mathrm{d}t. \tag{25}$$

From Eq. (25), we find the asymptotic expression for wall temperature distribution for $Pe_{\text{eff}} \gg 1$:

$$\lim_{\eta \to 0}[\Theta(\eta)] = \frac{3^{\frac{2}{3}} Pe_{\text{eff}}^{-\frac{1}{3}} Z^{\frac{1}{3}}}{2\Gamma[\frac{2}{3}]}. \tag{26}$$

Having the solutions for $\Theta$ with the respective boundary conditions, we substitute them into Eq. (15) and calculate the first-order correction to the pressure drop. In the next section, we compare the first-order correction to the pressure drop obtained from the Lévêque approach to the predictions for $\Delta P_1$ based on the numerical results for the temperature distribution found in the previous section.

## VI. FIRST-ORDER PRESSURE DROP CORRECTION FOR DIFFERENT BOUNDARY CONDITIONS

Temperature and viscosity in our problem are both scaled with reference to the entrance temperature $T_0$ and viscosity $\mu_0$. We consider that the entrance temperature at $Z = 0$, $T_0$, is lower than the temperature at the wall, $T_w$. Consequently, the average viscosity of the fluid is highest at the inlet and decreases as the fluid flows through the pipe. Therefore, we expect that any applied heating will cause a decrease in fluid viscosity resulting in a reduction in the overall pressure drop. Recall that the total pressure drop $\Delta P = \Delta P_0(1 + \beta\overline{\Delta P_1}....)$ where $\beta$ is a positive constant less than 1. We observe that $\overline{\Delta P_1}$, shown in Fig. 6, is negative, thus confirming a decrease in total pressure drop regardless of the nature of the applied heating investigated in this work. At small values of effective Peclet number, radial conduction dominates, leading to higher average temperatures, which correspond to lower average viscosities. In this regime, we observe the most significant decrease in the pressure drop. For $Pe_{\text{eff}} \ll 1$, we have $\Theta \approx 1$ and $\Theta \approx Z$ in the case of constant and linear applied boundary conditions, respectively. Therefore, in this limit, from Eq. (15), we expect the solution for $\overline{\Delta P_1}$ to approach $-1$ and $-1/2$ asymptotes, as the Graetz solution curves show in Fig. 6(a). Increasing the effective Peclet number corresponds to decreasing the thickness of a thermal boundary layer as cooler fluid rapidly advects through the channel. As a result, the average fluid temperature is lower and the average fluid viscosity is higher as compared to the small effective Peclet number limit. This provides insight into why we observe that the reduction in the total pressure drop is less at higher $Pe_{\text{eff}}$.

The applied linear boundary condition produces a lower average temperature field than that of the corresponding Dirichlet boundary condition at the wall for a given $Pe_{\text{eff}}$. Thus, in Fig. 6(a), we observe a smaller reduction in pressure drop for the linear boundary condition as compared to the constant temperature boundary condition for the entire range of $Pe_{\text{eff}}$. Also, from Fig. 6(a), we can ascertain that the Lévêque approximation converges well with the Graetz solution curves at high values of $Pe_{\text{eff}}$, as expected. In particular, for $Pe_{\text{eff}} \geq 25$, the error is less than 7%,

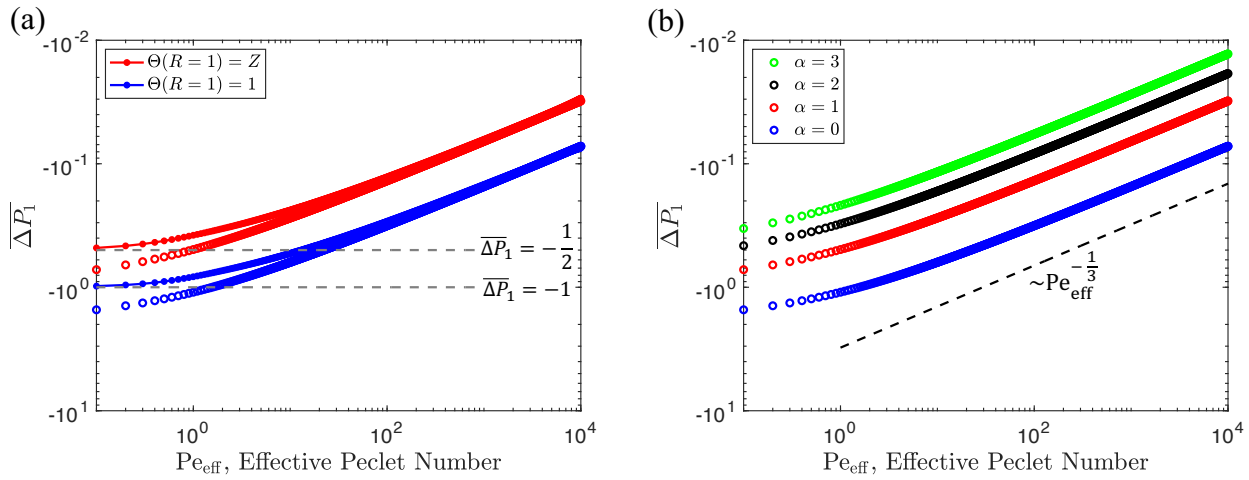


FIG. 6. (a) Normalized first-order pressure drop correction versus effective Peclet number curves for constant and linear applied boundary conditions. Dotted curves represent the results obtained from the Graetz solution to the temperature field whereas circles represent the results obtained from the Lévêque approximation. Gray dashed lines represent the low-$Pe_{\mathrm{eff}}$ asymptotes. (b) Normalized first-order pressure drop correction versus effective Peclet number curves for different powers $\alpha$ of $Z^{\alpha}$ obtained from the Lévêque approximation. The black dashed line represents the high-$Pe_{\mathrm{eff}}$ scaling $Pe_{\mathrm{eff}}^{-\frac{1}{3}}$.

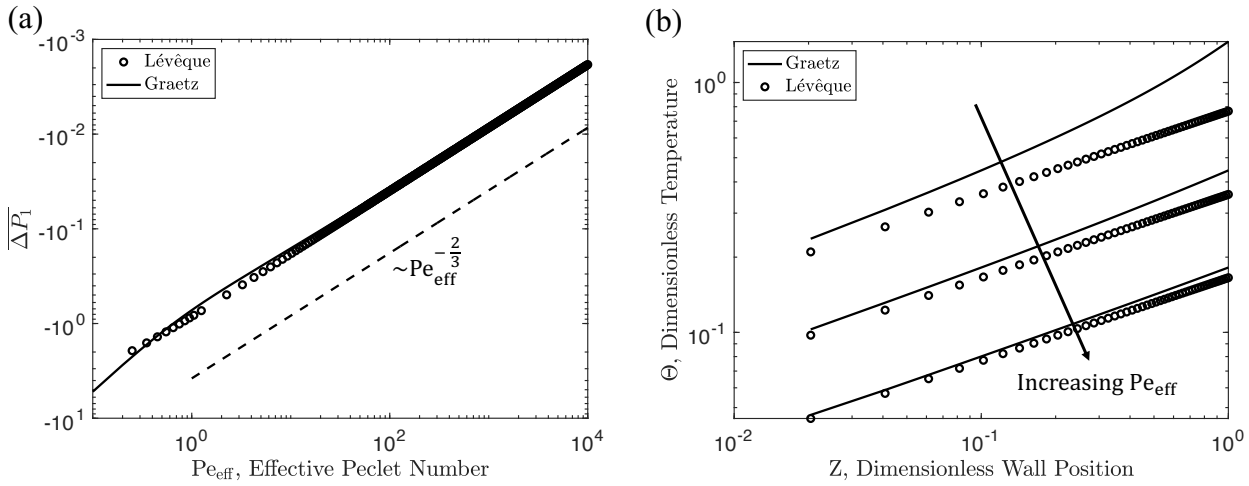


FIG. 7. (a) Normalized first-order pressure drop versus effective Peclet number curves for constant flux boundary condition at the wall. The solid curve represents the results obtained from the Graetz solution to the temperature field, the circles represent the Lévêque approximation and the black dashed line represents the high-$Pe_{\mathrm{eff}}$ scaling $Pe_{\mathrm{eff}}^{-\frac{2}{3}}$. (b) Wall temperature distribution for different effective Peclet numbers: $Pe_{\mathrm{eff}} = 1, 10, 100$. Solid curves represent the results obtained from the Graetz solution to the wall temperature whereas circles represent the Lévêque solution to the wall temperature from Eq. (26).

which provides further validation to this simplified method. In Fig. 6(b), we present our results of the normalized first-order pressure drop correction as a function of effective Peclet number for different powers $\alpha$ of $Z^{\alpha}$ using the Lévêque approach for constant, linear, quadratic, and cubic applied boundary conditions at the wall. Consistent with our previous results, we observe that as $\alpha$ increases, the average temperature in the flow field decreases, leading to a reduction in the normalized first-order pressure drop correction for a given $Pe_{\mathrm{eff}}$. Furthermore, it is evident from Fig. 6 that in the $Pe_{\mathrm{eff}} \gg 1$ limit, for all prescribed wall temperature conditions, the normalized first-order pressure drop correction scales as $\overline{\Delta P_1} = O\left(Pe_{\mathrm{eff}}^{-\frac{1}{3}}\right)$. Since Eq. (15) implies $\overline{\Delta P_1} = O(\Theta Y)$, and $\Theta = O(1)$ at most near the wall which gives, $\overline{\Delta P_1} = O(Y) = O\left(Pe_{\mathrm{eff}}^{-\frac{1}{3}}\right)$. This result is consistent with the aforementioned idea that the boundary layer thickness, $Y$, sets the average temperature in the fluid, which is directly related to the reduction in the pressure drop for the boundary conditions considered in Fig. 6.

Moreover, for a constant flux boundary condition at the wall, the average temperature distribution strongly depends on the value of the effective Peclet number since the wall temperature is not prescribed but determined from the balance between axial advection and radial conduction, as explained in Sec. V B. In Fig. 7(b) we show the wall temperature (where the temperature in the fluid is maximum), as a function of wall position for different effective Peclet numbers. We see that lower effective Peclet numbers yield higher wall temperatures and as $Pe_{\text{eff}}$ is increased, the Graetz solution for the wall temperature matches the Lévêque curve, Eq. (26), more closely, as shown in Fig. 7(b). Accordingly, in Fig. 7(a), we observe that $\overline{\Delta P_1}$ has a stronger dependence on the effective Peclet number at lower values compared to the previously discussed cases of constant and linear applied boundary conditions. In the high-$Pe_{\text{eff}}$ limit, it is evident from Fig. 7(a) that the normalized first-order pressure drop correction scales as $\overline{\Delta P_1} = O\left(Pe_{\text{eff}}^{-\frac{2}{3}}\right)$. From Eq. (26), we can ascertain that $\Theta = O(Y)$, while from Eq. (15) it follows that $\overline{\Delta P_1} = O(\Theta Y)$. Thus, we obtain that $\overline{\Delta P_1} = O(Y^2) = O\left(Pe_{\text{eff}}^{-\frac{2}{3}}\right)$ for $Pe_{\text{eff}} \gg 1$.

## VII. CONCLUDING REMARKS

In this work, we provided a general method that relies on the Lorentz reciprocal theorem to calculate the leading-order correction to the pressure drop for an axisymmetric channel flow with viscosity gradients produced by heating along the boundary. Assuming the fractional change in viscosity with temperature is small, we linearized the viscosity field and bypassed the complexity of solving the coupled interaction between velocity and temperature fields. Specifically, we found the temperature distribution and used it to find the leading-order correction to the pressure drop. The presented results provide insight into how the nature of the applied boundary condition affects the temperature-induced viscosity dependence on the pressure drop since, in many applications, the temperature at a channel wall may be non-uniform.

Our theoretical approach is not limited to the case of axisymmetric configurations and can be applied to rectangular geometries as well. As a future direction, it would be interesting to combine the present approach with the work of Boyko and Stone [25] to calculate the pressure drop dependence on effective Peclet number in heated, narrow channels of arbitrary shape. Finally, while we considered Newtonian fluids, it would be interesting to extend this work to complex fluids, such as polymer solutions and melts, where the interplay between viscous heating and non-Newtonian rheology may bring forth new insights.

## ACKNOWLEDGMENTS

This work was initiated while E.B. was working with H.A.S. at Princeton University. At that time, E.B. was supported by the Yad Hanadiv (Rothschild) Foundation and the Zuckerman STEM Leadership Program. E.B. acknowledges the support by grant no. 2022688 from the US-Israel Binational Science Foundation (BSF) in the late stages of this work. H.A.S. acknowledges the support from grant no. CBET-2246791 from the United States National Science Foundation (NSF).

[1] J. A. Whitehead and K. R. Helfrich, Instability of flow with temperature-dependent viscosity: A model of magma dynamics, J. Geophys. Res. **96**, 4145 (1991).
[2] J. J. Wylie and J. R. Lister, The effects of temperature-dependent viscosity on flow in a cooled channel with application to basaltic fissure eruptions, J. Fluid Mech. **305**, 239 (1995).
[3] K. Helfrich, Thermo-viscous fingering of flow in a thin gap: a model of magma flow in dikes and fissures, J. Fluid Mech. **305**, 219 (1995).
[4] A. Costa and G. Macedonio, Nonlinear phenomena in fluids with temperature-dependent viscosity: An hysteresis model for magma flow in conduits, Geophys. Res. Lett. **29**, 40 (2002).
[5] A. Costa and G. Macedonio, Viscous heating effects in fluids with temperature-dependent viscosity: Triggering of secondary flows, J. Fluid Mech. **540**, 21 (2005).
[6] S. Diniega, S. E. Smrekar, S. Anderson, and E. R. Stofan, The influence of temperature-dependent viscosity on lava flow dynamics, J. Geophys. Res. **118**, 1516 (2013).
[7] D. Maza Quinones, *Pipeline flow of heavy oil with temperature-dependent viscosity*, Tech. Rep. (PUC-Rio, 2010).
[8] L. G. Leal, Particle motions in a viscous fluid, Annu. Rev. Fluid Mech. **12**, 435 (1980).
[9] N. Oppenheimer, S. Navardi, and H. A. Stone, Motion of a hot particle in viscous fluids, Phys. Rev. Fluids **1**, 014001 (2016).

[10] C. Datt and G. J. Elfring, Active particles in viscosity gradients, Phys. Rev. Lett. **123**, 158006 (2019).
[11] V. A. Shaik and G. J. Elfring, Hydrodynamics of active particles in viscosity gradients, Phys. Rev. Fluids **6**, 103103 (2021).
[12] S. Ziegler and A.-S. Smith, Hydrodynamic particle interactions in linear and radial viscosity gradients, J. Fluid Mech. **943**, A29 (2022).
[13] F. S. Warnakulasuriya and W. M. Worek, Heat transfer and pressure drop properties of high viscous solutions in plate heat exchangers, Int. J. Heat Mass Transf. **51**, 52 (2008).
[14] C. Giessler, U. Lange, and A. Thess, Nonlinear laminar pipe flow of fluids with strongly temperature-dependent material properties, Phys. Fluids **19** (2007).
[15] S. M. Richardson, Injection molding of thermoplastics: Freezing of variable-viscosity fluids. II. Developing flows with very low heat generation, Rheol. Acta **25**, 308 (1986).
[16] N. Galili, R. Takserman-Krozer, and Z. Rigbi, Heat and pressure effect in viscous flow through a pipe: I. General formulation and basic solution, Rheol. Acta **14**, 550 (1975).
[17] H. Ockendon and J. R. Ockendon, Variable-viscosity flows in heated and cooled channels, J. Fluid Mech. **83**, 177 (1977).
[18] S. M. Richardson, Flows of variable-viscosity fluids in ducts with heated walls, J. Non-Newtonian Fluid Mech. **25**, 137 (1987).
[19] J. R. A. Pearson, Variable-viscosity flows in channels with high heat generation, J. Fluid Mech. **83**, 191 (1977).
[20] H. Ockendon, Channel flow with temperature-dependent viscosity and internal viscous dissipation, J. Fluid Mech. **93**, 737 (1979).
[21] M. M. Denn, Pressure drop-flow rate equation for adiabatic capillary flow with a pressure- and temperature-dependent viscosity, Polym. Eng. Sci. **21**, 65 (1981).
[22] T. Sun, Variable-viscosity flow in heated and cooled channels with internal viscous dissipation, Adv. Polym. **8**, 1 (1988).
[23] P. Schäfer and H. Herwig, Stability of plane Poiseuille flow with temperature dependent viscosity, Int. J. Heat Transfer **36**, 17 (1993).
[24] H. Masoud and H. A. Stone, The reciprocal theorem in fluid dynamics and transport phenomena, J. Fluid Mech. **879**, P1 (2019).
[25] E. Boyko and H. A. Stone, Reciprocal theorem for calculating the flow rate–pressure drop relation for complex fluids in narrow geometries, Phys. Rev. Fluids **6**, L081301 (2021).
[26] E. Boyko and H. A. Stone, Pressure-driven flow of the viscoelastic Oldroyd-B fluid in narrow non-uniform geometries: analytical results and comparison with simulations, J. Fluid Mech. **936**, A23 (2022).
[27] L. Graetz, Uber die Warmeleitungsfahigheir von Flussingkeiten, Ann. Phys. **254**, 79 (1882).
[28] L. Graetz, Uber die Warmeleitungsfahigheir von Flussingkeiten, Ann. Phys. **261**, 337 (1885).
[29] J. Sellars, M. Tribus, and J. Klein, Heat transfer to laminar flow in a round tube or flat conduit-the Graetz problem extended, J. Fluid Eng. **78**, 441 (1985).
[30] A. S. Haase, S. J. Chapman, P. A. Tsai, D. Lohse, and R. G. Lammertink, The Graetz–Nusselt problem extended to continuum flows with finite slip, J. Fluid Mech. **764**, R31 (2015).
[31] M. Rosales-Vera, A Note on the Cartesian Graetz problem with viscous dissipation, Case Stud. Therm. Eng. **28** (2021).
[32] M. A. Leveque, Les lois de la transmission de chaleur par convection, Ann. Mines **13**, 201 (1928).